JAAS

RSC Publishing

PAPER

View Article Online
View Journal | View Issue

The effect of laser pulse duration on ICP-MS signal intensity, elemental fractionation, and detection limits in fs-LA-ICP-MS

Cite this: *J. Anal. At. Spectrom.*, 2013, **28**, 1781

Nicole L. LaHaye,* Sivanandan S. Harilal, Prasoon K. Diwakar and Ahmed Hassanein

Received 18th June 2013
Accepted 4th September 2013

DOI: 10.1039/c3ja50200g

www.rsc.org/jaas

We investigated the role that pulse width has on the analytical capabilities of laser ablation-inductively coupled plasma-mass spectrometry (LA-ICP-MS), specifically in the range of 40 fs to 300 ps. Three main results of LA-ICP-MS were examined: signal intensity or sensitivity, elemental fractionation or that the ablated aerosol is representative of the bulk, and detection limits of various elements in the samples. The samples used for this experiment were NIST glass standards, dielectrics that exhibit different ablation properties compared to metal targets. Our results demonstrate that in the range of 40 fs to 1 ps, negligible differences occur in signal intensity, elemental ratios, and detection limits. The U/Pb and U/Th ratios, which were examined to ensure limited fractionation, give comparable results at all pulse widths investigated.

Introduction

Ultrafast laser ablation (LA) is a widely used technique in a variety of fields, from analytical chemistry in the form of laser-induced breakdown spectroscopy (LIBS)[1] and laser ablation-inductively coupled plasma-mass spectrometry (LA-ICP-MS),[2] to pulsed laser deposition (PLD),[3] to micromachining.[4,5] LA-ICP-MS in particular is useful for many different applications and samples, including glasses,[6] metals and alloys,[7,8] geology,[9] archaeology,[6,10] biological samples,[11] radioactive waste analysis,[9] *etc.* The important parameters that affect LA-ICP-MS performance include sample composition, laser properties (wavelength, pulse energy, pulse duration, repetition rate, spot size), carrier gas type and flow rate, ablation cell design, and ICP torch properties.[12,13] However, even after optimization of all these parameters, LA-ICP-MS can still experience elemental fractionation and matrix effects. Elemental fractionation, or non-stoichiometric ICP-MS results, can occur during laser ablation, during transport from the ablation chamber to the ICP torch, and within the ICP torch itself. Investigation into causes and mitigation of elemental fractionation have been performed using various techniques, including semiquantitative analysis[14] and ICP torch simulations,[15] but further investigation is necessary to fully elucidate the causes.

Pulse width plays a critical role in LA. Fig. 1 shows the approximate time scales of laser energy absorption and ablation for both ns- and fs-LA in the presence of an ambient, along with the various processes that occur[16] which include laser absorption at the surface and material excitation, temperature rise and surface melting, ablation and plasma formation, laser-plasma interaction (for ns-LA), shock wave formation, and plume collapse (in cases with sufficiently high ambient pressure). There are significant differences between ns- and fs-LA, originating from the vast spread in laser pulse duration. As can be seen in Fig. 1, in fs-LA case, plasma will be formed after the end of the pulse, whereas in ns-LA plasma is formed during the laser pulse, with part of the pulse energy serving to reheat the plasma. Because of this heating, persistence of the plasma is found to be higher for ns-LA compared to fs-LA.[17] The laser-plasma interaction is strongly dependent on laser wavelength and hence excitation wavelength plays a major role in ns-LA. However, our recent results showed that excitation wavelength is also important for fs LA sample introduction in ICP-MS.[13] The particle generation through plume condensation happens in the μs–ms time scales. Long duration ns pulses are frequently used in LA-ICP-MS due to the commercial availability of the lasers, but sample melting and mixing, as well as redeposition of aerosol onto the sample surface, greatly affect the accuracy and precision of analysis.[2,18] However, the short time scale of fs-LA prevents any significant heating of the sample, reducing the thermal effects that occur during ns-LA.[19] The electron to ion energy transfer time (τ_{ei}) ranges from ~1 to 10's of ps depending on the sample and is of the same order as the heat conduction time (τ_{heat}), which is much longer than the pulse duration (t_p) in typical fs-LA ($\tau_{ei} \sim \tau_{heat} \gg t_p$).

Our previous measurements, performed with a brass sample, showed pulse width (40 fs–1 ps) did influence particle number density while the distribution remains unchanged. Laser pulse energy affected both the distribution as well as the particle number density. Significant particle size based elemental fractionation was also observed for all the pulse widths including femtosecond laser pulses.[20]

Center for Materials Under Extreme Environment, School of Nuclear Engineering, Purdue University, West Lafayette, IN 47907, USA. E-mail: nlahaye@purdue.edu

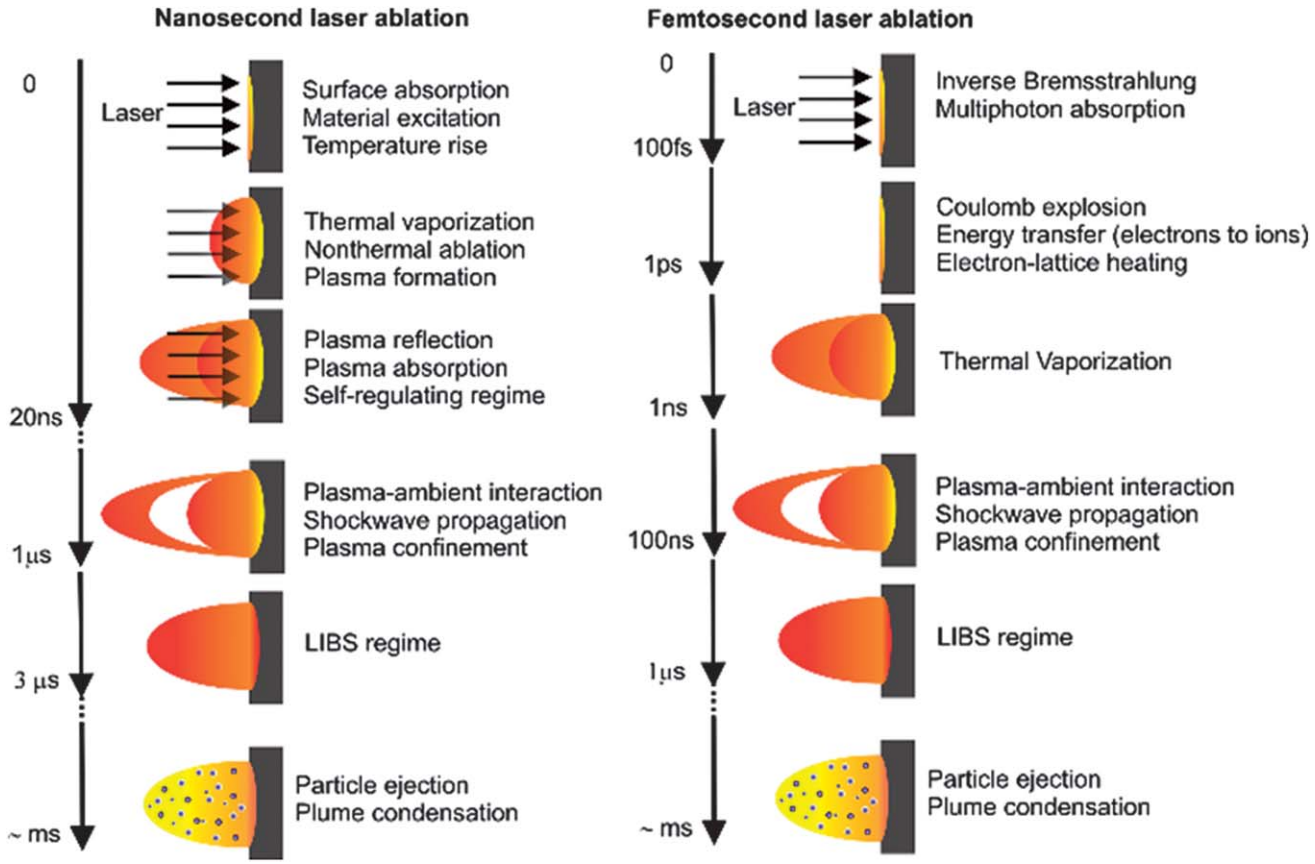

Fig. 1 Approximate time scales of laser energy absorption and ablation, along with the various processes that accompany it, for ns- and fs-LA in the presence of an ambient. 10 ns and 50 fs FWHM pulses were considered for ablation.

Energy transport in fs-LA happens in two distinct steps: energy absorption by electrons, ionizing the sample, and redistribution of energy to the lattice, causing material removal. In the range of fluences generally used for fs-LA-ICP-MS, ionization will occur either through collisional impact or multiphoton ionization. Collisional impact ionization (CII) occurs when free electrons collide with bound electrons, transferring energy and freeing the bound electrons.[21,22] Multiphoton ionization (MPI) occurs when multiple photons contribute enough energy to a valence electron to free it through excitation to metastable quantum states.[5,22,23] Coulomb explosion and thermal vaporization are the main mechanisms for material removal. In Coulomb explosion, free electrons form an electron cloud with a strong electric field, which serves to remove the ions from the bulk,[24] whereas in thermal vaporization, electron collisions increase the temperature of the sample, allowing for vaporization of material.[25]

Commercially available fs laser systems typically have pulse durations between 40 and 150 fs, but it is important to understand the effect that pulse widths closer to and greater than τ_{ei} and τ_{heat} have on LA and aerosol formation. Previous work has investigated the role of fs laser pulse width on ICP-MS analysis;[26,27] however, these works only investigated pulse width in the maximum range of 60 fs to 3 ps. In this paper the laser pulse duration was varied from 40 fs to 300 ps, showing the effect of pulse duration at values well below, around, and above τ_{ei} and τ_{heat}. We examined how the laser pulse width affects elemental fractionation, in addition to ICP-MS signal intensity and elemental detection limits.

Experimental

The experimental configurations of the fs laser system, beam delivery, and analyzer for fs-LA-ICP-MS are given elsewhere.[13,20] The Ti:Sapphire laser is a chirped pulse amplification (CPA)-based system (Amplitude Technologies), with output wavelength ~800 nm and repetition rate 10 Hz. The maximum output laser energy is ~10 mJ, but energy was reduced using a combination of half-wave plate and thin film polarizer to 400 μJ or 1 mJ for the purposes of these experiments. The spot size was kept constant throughout the experiments, so the only parameter that is changing is the power flux, due to the variation of the laser pulse width. An energy of 400 μJ was used for LA in the pulse width range 40 fs–1 ps. It is important to note that at 300 ps pulse width the laser energy is increased to 1 mJ to ensure that the laser fluence used in the experiment is well above the ablation threshold for all pulse widths used, so no threshold phenomena are observed.[13] Energy variation of the laser was below 2%. Pulse duration of the laser is variable from 40 fs to 1 ps through adjustment of the compressor grating, with

Table 1 Concentration (in ppm) of the elements analyzed in this study for NIST SRMs 610, 613, 615, and 616

Sample	Fe	Cu	Sr	Pb	Th	U
SRM-610	458 ± 9	444 ± 4	515.5 ± 0.5	426 ± 1	457.2 ± 1.2	461.5 ± 1.1
SRM-613	51 ± 2	37.7 ± 0.9	78.4 ± 0.5	38.57 ± 0.2	37.79 ± 0.08	37.38 ± 0.08
SRM-615	13.3 ± 1.0	1.37 ± 0.07	45.8 ± 0.1	2.32 ± 0.04	0.748 ± 0.006	0.823 ± 0.02
SRM-616	11 ± 2	0.80 ± 0.09	41.72 ± 0.05	1.85 ± 0.04	0.0252 ± 0.0007	0.0721 ± 0.0013

additional pulse duration of 300 ps attainable through bypassing the compressor. Laser pulse duration was measured using an auto-correlator.

A series of high-reflecting mirrors transport the beam to the ablation chamber (J100 Series, Applied Spectra), with an objective lens focusing the laser down to ~75 μm spot size on the target. The ablation chamber is mounted on an *XYZ* translation stage, allowing for movement of the target, and a CCD camera mounted above the chamber allowed for visualization and focusing. Single spot ablation mode was used for these experiments to avoid surface effects; however, this will affect ablation rate and elemental fractionation, as both are dependent on crater formation. Four different NIST standard reference materials (SRMs) were used (610, 613, 615, and 616), and the following isotopes were analyzed: ^{56}Fe, ^{63}Cu, ^{65}Cu, ^{88}Sr, ^{208}Pb, ^{232}Th, ^{235}U, and ^{238}U (concentrations given in Table 1). Argon was used as carrier gas, flowing at 1 L min^{-1}, and the ablation chamber was connected to the ICP-MS using Tygon tubing. Important experimental parameters are summarized in Table 2.

The aerosol was analyzed using a quadrupole-based ICP-MS (ICP-MS 7700×, Agilent Technologies Inc.), operating at 1550 W and without use of the collision cell. Transient analysis mode was employed, with duration of 90 seconds; the first ten seconds were blank, followed by 50 seconds with the laser triggered, then finally 30 seconds of washout. The first few seconds of signal (after initial laser triggering) were ignored so that surface effects can be neglected. Data processing was performed by averaging five seconds of signal. The ICP-MS operating conditions were optimized prior to the start of each experiment.

Table 2 Summary of important laser and ICP-MS experimental parameters, in addition to a list of samples used, for fs-LA-ICP-MS

Experimental parameters	
Laser system/beam delivery	
Wavelength	~800 nm
Pulse duration	40 fs–300 ps
Energy	400 μJ, 1 mJ
Repetition rate	10 Hz
Beam diameter	10 mm
Spot size	~75 μm
Fluence	9–23 J cm^{-2}
Angle of incidence	Normal to the target
Objective lens NA	0.13
Sampling mode	Single spot
ICP-MS	
Torch RF power	1550 W
Carrier gas	1.0 L min^{-1} Ar
Gas through torch	15 L min^{-1} Ar
Integration time per isotope	20 ms
Dwell time	180 ms
Sample material	
Silicate glass	NIST SRM 610, 613, 615, 616
Isotopes analyzed	^{56}Fe, ^{63}Cu, ^{65}Cu, ^{88}Sr, ^{208}Pb, ^{232}Th, ^{235}U, ^{238}U

Results and discussion

The purpose of this work was to investigate the role that pulse width has on the analytical capabilities of LA-ICP-MS, specifically in the range of 40 fs to 300 ps. The ICP-MS signal intensity, elemental fractionation, and detection limits were studied. The pulse widths selected ranged from shorter to longer than the electron-ion relaxation time; the laser-target coupling, laser-plasma coupling as well as ablation mechanisms will therefore vary as a function of pulse width, allowing for a better understanding of the effect of pulse width on LA.

Pulse width effect on ICP-MS signal

To study how pulse width affects LA rate, ICP-MS signal was monitored for a variety of elements with ablation at a constant energy of 400 μJ, constant fluence of 9 J cm^{-2} for pulse widths between 40 fs and 1 ps, and 1 mJ energy, fluence 23 J cm^{-2} at 300 ps. The laser fluences used in the present work is significantly higher than the ablation threshold values reported for glass samples for various pulse widths, theoretically calculated to be 2 J cm^{-2} below 1 ps and ~21 J cm^{-2} at 300 ps.[28] The eight isotopes detected range from low to high mass (^{56}Fe, ^{63}Cu, ^{65}Cu, ^{88}Sr, ^{208}Pb, ^{232}Th, ^{235}U, and ^{238}U). The sum of their signals *vs.* time at various pulse widths is displayed in Fig. 2; the signal is approximately constant for pulse widths between 40 fs and 1 ps, with a decrease of only a factor of two between the two extremes, while the signal at 300 ps is only comparable to the other pulse widths due to the increase in laser energy. This indicates that the ablation rate is approximately constant for 40 fs to 1 ps pulse durations, but is lower for t_p = 300 ps. Freydier *et al.* also reported similar results for pulse widths between 60 fs and 3 ps.[27] The signal shape is identical for 40–700 fs pulse widths, while the signal shapes for 1 ps and 300 ps showed some similarities. The differences in temporal features of ICP-MS signal with respect to pulse width can be due to a few different effects, including changes in power flux and thermal induced effects, and has been previously observed in LA of brass samples[20] and in NIST 612.[27] The difference in signal background as a function of pulse width has also been previously observed and is thought to be due to

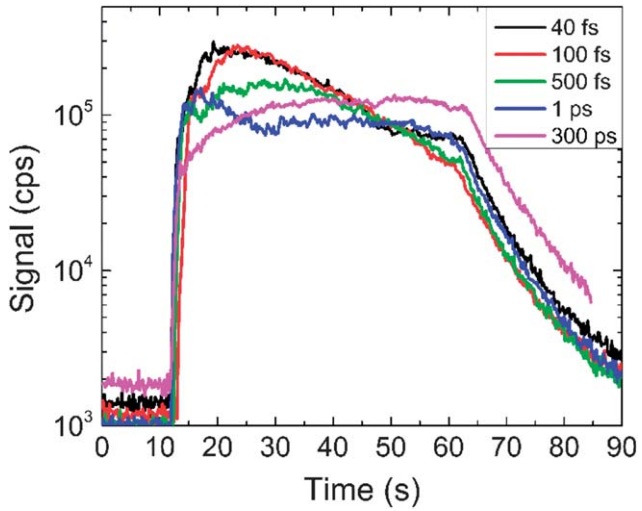

Fig. 2 ICP-MS signal intensity *vs.* time for fs-LA-ICP-MS analysis of NIST 610, for various pulse widths, using Ti:Sapphire laser with ~800 nm wavelength at 400 μJ energy for pulse widths 40 fs–1 ps, 1 mJ energy for 300 ps.

memory effects due to accumulation of sample on the introduction interface.[26] Fig. 3 shows the signal for the four different samples used in this experiment at laser pulse width of 100 fs. The results shown are what is expected based on the relative concentration of the elements detected in each sample. The signal from NIST 615 and 616 are approximately equal, with NIST 613 signal an order of magnitude higher and NIST 610 two orders of magnitude higher than the NIST 616 signal. The agreement between bulk concentration and ICP-MS signal demonstrates that ablation rate is approximately constant for each sample, despite differences in opacity (NIST 610 is opaque, while NIST 613-616 are transparent).

To demonstrate the consistency of ICP-MS signal strength for pulse widths between 40 fs and 300 ps, the average ICP-MS signal intensity was plotted *vs.* time in Fig. 4. The average signal was calculated from 5 seconds of signal shortly after laser triggering, with initial signal ignored so that surface effects can be neglected. The average signal is approximately constant as pulse width increases from 40 fs to 1 ps; however, there is a small decrease in signal when the pulse width changes from 1 ps to 300 ps. This again demonstrates that ablation rate is approximately constant for pulse widths between 40 fs and 1 ps, with a difference occurring between 1 ps and 300 ps. Since the NIST sample predominantly contains SiO_2 and considering the electron-ion relaxation time of Si ~5 ps, the ablation efficiency will be more or less constant for pulse widths below τ_{ei}. For pulse widths well above characteristic relaxation times, the ablation mechanism changes from electric field-dominated to thermal ablation (characteristic of long pulse ablation).[28] Temporal relative standard deviation (TRSD) was also calculated for the 5 seconds used to compute the average signal. The TRSD is consistent for pulse widths between 40 fs and 1 ps, between 5 and 10%, but increases for higher pulse widths to values generally observed in ns-LA-ICP-MS. Minimal error can be achieved for pulse widths below 1 ps, where heating effects are minimized.

Sample material will have a great effect on the influence of pulse width. Fig. 5 compares NIST 610 LA-ICP-MS signal from this work to brass LA-ICP-MS signal from previous work.[20] Laser fluence for brass sample was 1.5 J cm^{-2} for all pulse widths, whereas laser fluence for NIST 610 was 9 J cm^{-2} for pulse widths 40 fs–1 ps and 23 J cm^{-2} for 300 ps. The data for each sample was normalized to the relative concentration of the elements analysed for ease of comparison. As can be seen in Fig. 5, brass gives lower signal levels and a much more constant response for pulse widths between 40 fs and 1 ps, in comparison with glass standard while the decrease in signal at 300 ps is more drastic because similar fluence was used for all brass measurements. Signal is lower for brass due to use of a lower laser fluence and

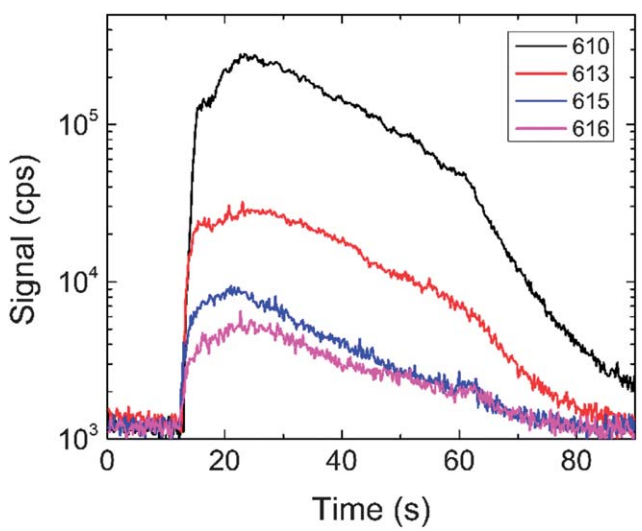

Fig. 3 ICP-MS signal intensity *vs.* time, 100 fs laser pulse width, 400 μJ energy, for fs-LA-ICP-MS analysis of each NIST sample.

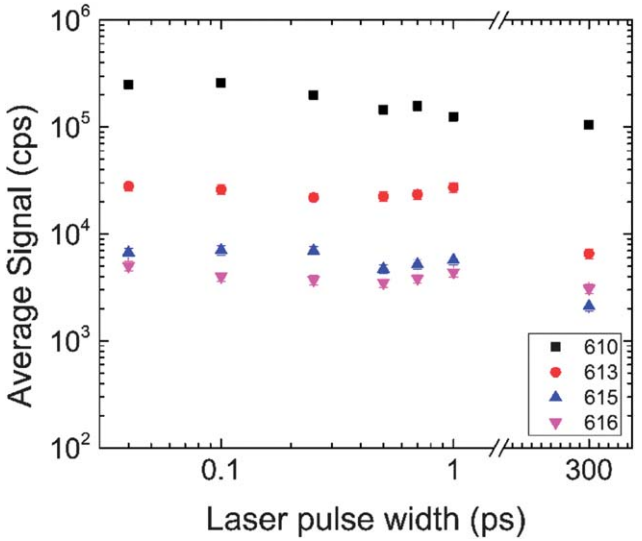

Fig. 4 Average signal *vs.* pulse width for all four NIST samples at 400 μJ laser energy.

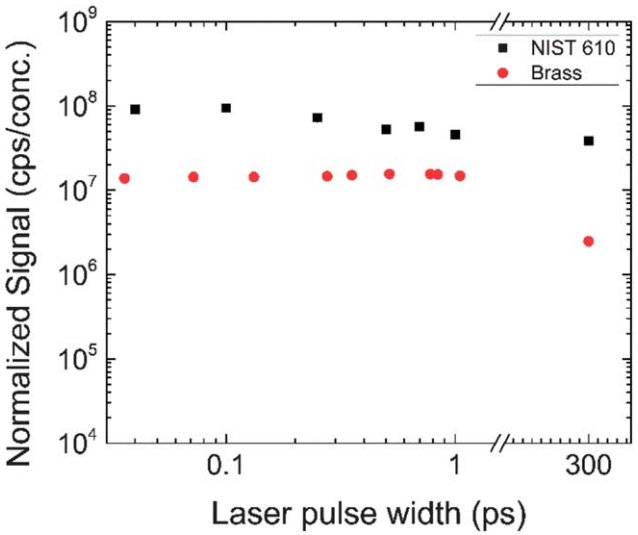

Fig. 5 Comparison of ICP-MS signal *vs.* pulse width for brass sample and NIST 610 glass standard. Laser fluence for brass sample was 1.5 J cm^{-2} for all pulse widths; laser fluence for NIST 610 was 9 J cm^{-2} for pulse widths 40 fs–1 ps and 23 J cm^{-2} for 300 ps. Brass signal is comprised of ^{65}Cu signal; NIST 610 signal is a sum of the 8 isotopes analyzed. Data is normalized to elemental concentration in each sample.

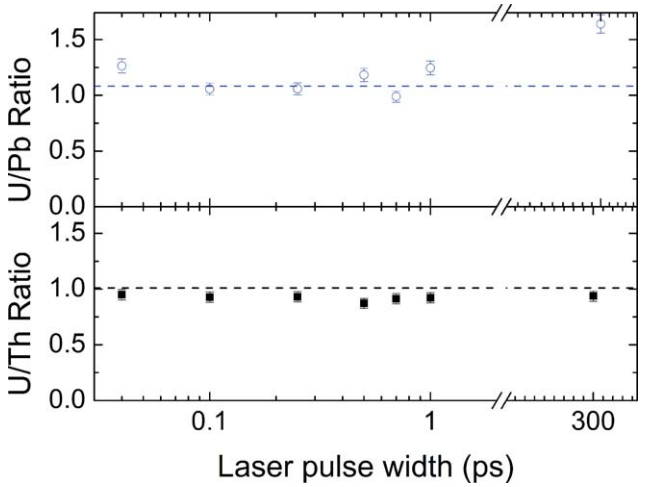

Fig. 6 U/Th and U/Pb ratio for NIST 610. Expected value for U/Th ratio is 1.009 and for U/Pb ratio is 1.083, indicated by the dashed lines.

differences in ablation mechanisms associated with metal and dielectric targets. This phenomena is explained well by Gamaly *et al.*[28] Since LA for t_p less than τ_{ei} and τ_{heat} is electric field-motivated, free electron density is of extreme importance. In a metal, these free electrons are readily available; in a dielectric (such as NIST 610 used here), energy is needed to promote electrons from the conduction to the valence band. This promotion of electrons is dependent upon the laser energy and time of interaction. Because the same energy was used at all pulse widths, the only variable is the time of interaction, or the laser pulse duration. Increased laser power flux (*i.e.*, decreased pulse width) will create more free electrons, which will in turn create a stronger electric field.

Elemental fractionation

Elemental fractionation is a very important consideration for LA-ICP-MS. By minimizing fractionation through laser and other parameters, it is possible to attain non-matrix-matched calibration, which is especially important in samples where the matrix is unknown or there does not exist a calibrated, matrix-matched standard. Non-matrix-matched calibration has been previously demonstrated for pulse widths ~100 fs, but is very difficult to obtain for ns-LA.[8] However, it is important to understand the influence of pulse width in a wide range.

One way to measure elemental fractionation is through detection of elemental ratios as a function of some parameter, in this case, laser pulse duration. The U/Th and U/Pb ratios in particular are a measure of laser- and transport-induced elemental fractionation,[29] which are the two aspects of elemental fractionation that are of greatest interest here. Fig. 6 show U/Th and U/Pb ratios, as a function of pulse width in the range 40 fs to 300 ps for LA of NIST 610. U/Th ratio results are consistent, with the results at all pulse widths within ~10% of the expected ratio of 1.009, indicated by a dashed line on the plot. Similarly, the U/Pb ratio results also match the expected ratio of 1.083 at pulse widths between 40 fs and 1 ps, within ~10% variation, but is much higher than the expected ratio at 300 ps pulse width. This indicates that pulse width-induced elemental fractionation does not occur in the range of 40 fs to 1 ps, whereas at 300 ps, sample heating affects the U/Pb ratio. The close match to the expected ratio at all pulse widths gives evidence that, for the laser parameters used here, similar samples could be calibrated without perfectly matrix-matched samples.

Calibration and detection limits

Standard reference materials, such as NIST 610-616 used in this study, are commonly used to accurately quantify elemental concentrations[7] in samples where elemental content and concentration is unknown. This is done through the use of calibration curves, such as the calibrations curves for U at four different pulse widths that are seen in Fig. 7. As the four NIST SRMs used in this experiment contain different concentrations of the different elements examined (see Table 1), plotting ICP-MS signal *vs.* concentration of the element in the sample and performing a linear fit provides a way to calculate the concentration of a certain element in an unknown sample from the detected ICP-MS signal.

Another use for calibration plots is to calculate detection limits, or the minimal concentration of a given element that can be distinguished from background signal. Here, detection limits are calculated as:

$$\text{Detection limit} = 3\sigma_b/s \quad (1)$$

where σ_b is the standard deviation of the background signal and s is the slope of the calibration curve for the element in question. The detection limits of Pb and U as a function of pulse width are given in Fig. 8. Detection limits follow a linear trend

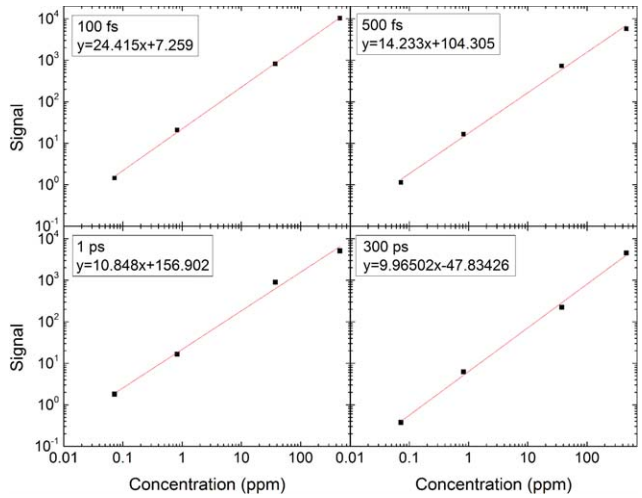

Fig. 7 Calibration plots for U at 100 fs, 500 fs, 1 ps, and 300 ps laser pulse widths.

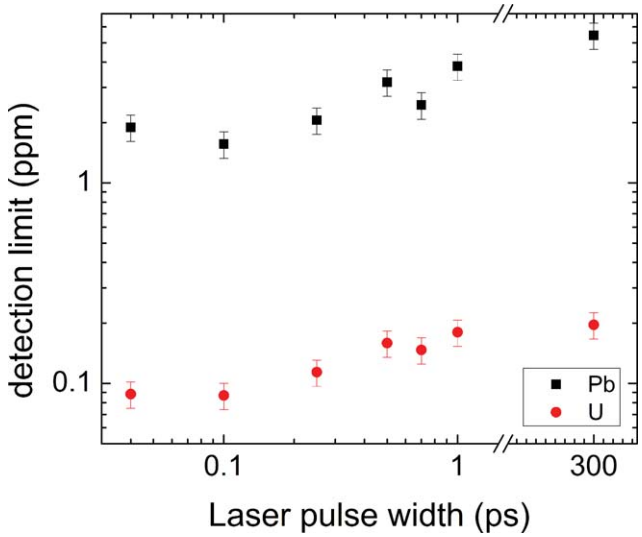

Fig. 8 Detection limits for Pb and U *vs.* laser pulse width.

as a function of pulse width, with the increase in detection limit being higher for Pb than for U. U detection limit increases from ~0.07 ppm at 40 fs to ~0.2 ppm at 300 ps (1.5 orders of magnitude), whereas Pb detection limit increases from ~1 ppm at 40 fs to ~5 ppm at 300 ps. This indicates that for applications where trace element detection is necessary, it is preferable to use the shortest pulse width attainable. The results above show very little difference in signal intensity and elemental ratio in the range of 40 fs to 1 ps, but detection limits show, in the case of uranium, a ~50% increase in detection limits from 40 fs to 1 ps, which can be crucial in trace element analysis.

Conclusions

We investigated the pulse width effect on laser ablation particle generation through ICP-MS signal response, U/Th and U/Pb elemental ratios, and elemental detection limits. Laser pulse widths were varied from 40 fs, which is considerably lower than characteristic energy transfer times, to 300 ps, well above those characteristic times. The ICP-MS response to LA with laser pulse widths in the range of 40 fs to 300 ps was examined to study changes in ablation rate. For pulse widths between 40 fs and 1 ps, ICP-MS signal was approximately constant; however, there was a decrease in signal as pulse width increased from 1 ps to 300 ps. A comparison of NIST 610 to brass sample showed that metals have a more consistent response between 40 fs and 1 ps. TRSD is also approximately constant between 40 fs and 1 ps, and is lower at these pulse widths than at 300 ps.

The U/Th and U/Pb ratios also match the expected value well across the entire range of pulse widths studied, except for U/Pb at 300 ps. This shows that under the conditions used in this study, elemental fractionation is minimized as a function of pulse width, an important result for studies in which non-matrix-matched calibration would be employed. Detection limits were also calculated through the use of calibration curves. The lowest detection limits were achieved at 40 fs, with a linear increase in detection limit as pulse width increased. In applications where trace element detection is important, it is best to use the shortest pulse width available, as lower detection limits will allow accurate determination of elements even in the ppb range.

Acknowledgements

This work is partially supported by U.S. Department of Energy, office of National Nuclear Security Administration under award number DE-NA0000463.

Notes and references

1 J. Singh and F. Yueh, *Lasers & Electro-Optics & the Pacific Rim Conference on Lasers and Electro-Optics*, vol. 1 and 2, 2009, p. 456.
2 J. Koch and D. Gunther, *Appl. Spectrosc.*, 2011, **65**, 155a.
3 S. Heiroth, J. Koch, T. Lippert, A. Wokaun, D. Gunther, F. Garrelie and M. Guillermin, *J. Appl. Phys.*, 2010, **107**, 014908.
4 R. Degl'Innocenti, S. Reidt, A. Guarino, D. Rezzonico, G. Poberaj and P. Gunter, *J. Appl. Phys.*, 2006, **100**, 113121.
5 X. Liu, D. Du and G. Mourou, *IEEE J. Quantum Electron.*, 1997, **33**, 1706.
6 V. S. Selih and J. T. van Elteren, *Anal. Bioanal. Chem.*, 2011, **401**, 745.
7 V. Mozna, J. Pisonero, M. Hola, V. Kanicky and D. Gunther, *J. Anal. At. Spectrom.*, 2006, **21**, 1194.
8 J. Gonzalez, C. Liu, X. Mao and R. Russo, *J. Anal. At. Spectrom.*, 2004, **19**, 1165.
9 R. E. Russo, X. L. Mao, H. C. Liu, J. Gonzalez and S. S. Mao, *Talanta*, 2002, **57**, 425.
10 L. B. Brostoff, J. J. Gonzalez, P. Jett and R. E. Russo, *J. Archaeol. Sci.*, 2009, **36**, 461.
11 J. Becker, M. Zoriy and M. Przybylski, *J. Anal. At. Spectrom.*, 2007, **22**, 63; C. Austin, T. M. Smith, A. Bradman,

K. Hinde, R. Joannes-Boyau, D. Bishop, D. J. Hare, P. Doble, B. Eskenazi and M. Arora, *Nature*, 2013, **498**, 216.
12 C. C. Garcia, H. Lindner and K. Niemax, *J. Anal. At. Spectrom.*, 2009, **24**, 14.
13 N. L. LaHaye, S. S. Harilal, P. K. Diwakar, A. Hassanein and P. Kulkarni, *J. Appl. Phys.*, 2013, **114**, 023103.
14 A. Leach and G. Hieftje, *Anal. Chem.*, 2001, **73**, 2959.
15 L. Flamigni, J. Koch and D. Gunther, *Spectrochim. Acta, Part B*, 2012, **76**, 70; F. Vanhaecke, R. Dams and C. Vandecasteele, *J. Anal. At. Spectrom.*, 1993, **8**, 433.
16 M. Sabsabi, in *Laser-Induced Breakdown Spectroscopy*, ed. J. P. Singh and S. N. Thakur, Elsevier, Amsterdam, 2007; E. Gurevich and R. Hergenroder, *Appl. Spectrosc.*, 2007, **61**, 233A; B. Rethfeld, K. Sokolowski-Tinten, D. von der Linde and S. Anisimov, *Appl. Phys. A: Mater. Sci. Process.*, 2004, **79**, 767; A. E. Hussein, P. K. Diwakar, S. S. Harilal and A. Hassanein, *J. Appl. Phys.*, 2013, **113**, 143305.
17 J. Freeman, S. S. Harilal, P. K. Diwakar, B. Verhoff and A. Hassanein, *Spectrochim. Acta, Part B*, 2013, **87**, 43–50.
18 B. Verhoff, S. S. Harilal and A. Hassanein, *J. Appl. Phys.*, 2012, **111**, 123304.
19 L. Zhu, G. Gamez, T. A. Schmitz, F. Krumeich and R. Zenobi, *Anal. Bioanal. Chem.*, 2010, **396**, 163.
20 P. K. Diwakar, S. S. Harilal, N. L. LaHaye, A. Hassanein and P. Kulkarni, *J. Anal. At. Spectrom.*, 2013, **28**, 1420.
21 K. Wong, S. Vongehr and V. V. Kresin, *Phys. Rev. B: Condens. Matter Mater. Phys.*, 2003, **67**, 035406.
22 A. Kaiser, B. Rethfeld, M. Vicanek and G. Simon, *Phys. Rev. B: Condens. Matter Mater. Phys.*, 2000, **61**, 11437.
23 D. Arnold and E. Cartier, *Phys. Rev. B: Condens. Matter Mater. Phys.*, 1992, **46**, 15102.
24 X. W. Wang and X. F. Xu, *J. Heat Transfer*, 2002, **124**, 265; H. P. Cheng and J. D. Gillaspy, *Phys. Rev. B: Condens. Matter Mater. Phys.*, 1997, **55**, 2628; R. Stoian, D. Ashkenasi, A. Rosenfeld and E. E. B. Campbell, *Phys. Rev. B: Condens. Matter Mater. Phys.*, 2000, **62**, 13167.
25 E. N. Glezer, Y. Siegal, L. Huang and E. Mazur, *Phys. Rev. B: Condens. Matter Mater. Phys.*, 1995, **51**, 9589; A. Miotello and R. Kelly, *Appl. Phys. A: Mater. Sci. Process.*, 1999, **69**, S67; M. Toulemonde, C. Dufour, A. Meftah and E. Paumier, *Nucl. Instrum. Methods Phys. Res., Sect. B*, 2000, **166**, 903.
26 F. d'Abzac, F. Poitrasson, R. Freydier and A. Seydoux-Guillaume, *J. Anal. At. Spectrom.*, 2010, **25**, 681.
27 R. Freydier, F. Candaudap, F. Poitrasson, A. Arbouet, B. Chatel and B. Dupre, *J. Anal. At. Spectrom.*, 2008, **23**, 702.
28 E. Gamaly, A. Rode, B. Luther-Davies and V. Tikhonchuk, *Phys. Plasmas*, 2002, **9**, 949.
29 J. Koch, M. Walle, J. Pisonero and D. Gunther, *J. Anal. At. Spectrom.*, 2006, **21**, 932.